# Large Eddy Simulations of Turbulence under Internal Solitary Waves of Depression

Takahiro Sakai [(1)] , Peter J. Diamessis [(2)] and Gustaaf B. Jacobs [(3)]

(1) Department of Aerospace and Mechanical Engineering,
University of Southern California, Los Angles, CA 90089-1191, U.S.A.
tsakai@usc.edu

(2) School of Civil and Environmental Engineering,
Cornell University, Ithaca, NY 14853, U.S.A.
pjd38@cornell.edu

(3) Department of Aerospace Engineering and Engineering Mechanics,
San Diego State University, San Diego, CA 92182, U.S.A.
gjacobs@mail.sdsu.edu

## Abstract

The bottom boundary layer (BBL) under an internal solitary wave (ISW) of depression is examined using highly resolved, spectral multidomain penalty-method based, Large Eddy Simulation. The focus is on the three-dimensionalization of the initial shear-instability-driven near-bed vortex wake in the lee of the wave and on the downstream formation of fully developed turbulence. When the ISW propagates into quiescent water, the near-bed vortex wake forms only when the separated BBL is persistently perturbed in the form of localized volumetric forcing. In addition, the near-bed wake three-dimensionalizes but does not become turbulent. When the ISW encounters an oncoming barotropic current, a spontaneous (no perturbations required) complex structural transition to turbulence gives rise to a fully turbulent self-sustained near-bed wake upstream of the wave. Preliminary quantitative results on the turbulent BBL serve as the springboard for a more detailed forthcoming study.

## 1. Introduction

Internal solitary waves (ISWs) transport energy $O$(100km) distances from their actual generation sites before dissipating it. A critical component of the transport and dissipation of energy by propagating ISWs is their interaction with the seafloor (Moum et al. 2007). The resulting turbulence and particulate resuspension are of particular importance to shelf energetics, ecology, water-quality, bed morphology acoustics and optics (e.g. Bogucki et al. 2005 ; Quaresma et al. 2007 ; Reeder and Ma 2011)

Focusing on ISWs of depression, it has been regularly hypothesized that the turbulence under ISWs directly results from a global instability of the separated bottom boundary layer (BBL) occurring in the lee of the wave (Diamessis and Redekopp 2006 ; see Stastna and Lamb 2008 for a discussion of elevation waves). The above hypothesis, in the context of the incipient 2-D instability, has repeatedly been confirmed by a number of 2-D Direct Numerical Simulation (DNS)-based investigations (see Aghsaee et al. 2012 for a review). In the overwhelming majority of these studies, the global instability is intimately connected to the formation of a separation bubble in the lee of the ISWs footprint due to the presence of an oncoming barotropic current. Laboratory studies, where no oncoming current is present, have reported the separation of the BBL under an ISW (Carr et al. 2008). Although no BBL reattachment is observed, vortex shedding was reported (Carr et al. 2008 ; Aghsaee and Boegman 2015). The latter of these two studies was the first to provide data on the full 3-D velocity field in the

ISW-induced BBL through timeseries of the transverse velocity obtained by a near-bed ADV. The full 3-D structure of the BBL under an ISW has only been documented for the case of a wave going over an isolated topographic bump (Harnanan et al. 2015 ; Soontiens et al. 2015). Any BBL instability (global or otherwise) in these studies is restricted to the time the ISW passes over the topographic feature and does not persist once the wave resumes its propagation over a flat bottom.

No controlled laboratory or numerical study exists which examines the persistent self-sustained near-bed turbulent wake, originating from a global instability, under an ISW over considerable propagation distances. Relying on ongoing, computationally costly, Large Eddy Simulations (LES), this paper's primary objective is to provide a preliminary set of results on the turbulence transition of the initial near-bed vortex wake and resulting turbulence near-bed wake for an ISW of depression.

## 2. Numerical Model

The computational domain is an elongated rectangular box with a continuous, two-layered tanh-stratification in which a base-state ISW of depression is situated against an oncoming, mean background barotropic current $U(z)$, as described in Figure 1. The frame of reference is fixed on the leftward propagating wave.

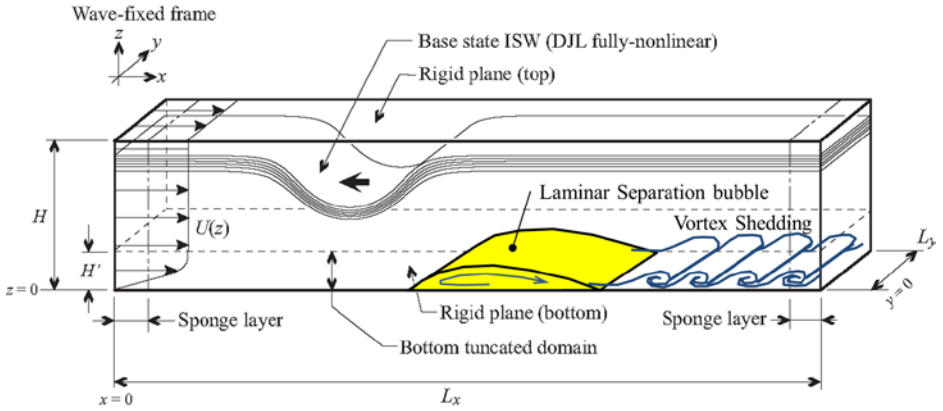


Figure 1: Model schematic.

The computational domain is chosen to have a depth of $H$=10 m, an along-wave length of $L_x$=260 m and a width of $L_y$=3 m. The pycnocline is centered at a depth of $H$/7.5 from the top surface, corresponding to an upper-to-lower-layer thickness ratio of 1/6.5, with a thickness of $H$/15. The ISW velocity and density fields are calculated by numerically solving the DJL equation (Dunphy et al. 2011). The resulting wave has a large amplitude, measured by the maximum wave-induced isopycnal displacement, of 0.346$H$ which corresponds to 86% of the corresponding conjugate state limit value (Lamb and Wan 1998) for the stratification at hand. The ISW wavelength is 2.33$H$ and the phase speed in the absence of a background current is $c_0$ = 0.8965 m/s which corresponds to 99% of the conjugate state limit value. The kinematic viscosity is chosen as $\nu = 5.56\times10^{-5}$ m$^2$/s. As such, the wave Reynolds number is $Re_W = (c+U_0)H/\nu = 1.6\times10^5$ ($c$ is a wave phase speed at the background current velocity $U_0$) which is comparable to the value employed by laboratory experiments (Carr et al. 2008).

The incompressible Navier-Stokes equations are formulated to have the wave and background current as a permanent base-state, and field variables are formulated as perturbations from the base-state (Diamessis and Redekopp 2006). This study is essentially a multi-scale problem, demanding high resolution of the BBL which extends many ISW wavelengths downstream of the wave trough: an initially laminar BBL undergoes a 2-D instability and then transitions to

turbulence. The scale separation between ISW and BBL in this study is about four orders of magnitude. To alleviate this stringent resolution requirement, the computational domain is truncated to the lower 30% of the water column reducing the domain's stream-to-depth aspect ratio value of 87. Since the ISW velocity and density fields are kept fixed in time and the truncated domain resides fully within the lower layer of the two-layer stratification, buoyancy effects do not directly impact the evolution of the BBL. Hence, the solution of the advection-diffusion equation for the density may be avoided to reduce computational cost. The computational domain is periodic in both streamwise and spanwise directions and has an impermeable, stress-free rigid top lid and an impermeable, no-slip rigid bed. Exploratory two-dimensional simulations, conducted prior to the full production runs, have shown that the computational domain is sufficiently tall to ensure that the wave-induced BBL, namely the structure of the separation bubble and its instability properties, remains nearly the same with the full water column case. A sponge layer is inserted at the forward ($x$=0), aft ($x$=$L_x$) and top boundaries to ensure a perturbation-free inflow and to suppress reflections that can potentially alter the flow in the domain interior. The wave trough is centered at $x$=60$m$, which provides 8.5 ISW wavelengths for the BBL flow to evolve downstream.

The high-accuracy/resolution MPI-parallelized flow solver of Diamessis et al. (2005), based on a spectral multi-domain spectral penalty method in the vertical, Fourier discretizations on the horizontal plane and stiffly-stable, high-order variable time stepping, is employed. Along with dealiasing, additional stabilization is enabled through application of a weak, exponential spectral filter (12th-order in horizontal and 14th-order in vertical) to suppress spurious energy build-up at the smallest resolved scales and ensure stable long-time integration.

Numerical resolution is chosen to be $N_x \times N_y \times N_z$ = 12288×128×480 (approximately 0.75 billion grid points). Twelve spectral subdomains are used in the vertical with 40 points each. The time step ranges from 0.00017 to 0.002. The grid resolution is compared to that used in published numerical investigations of aerodynamic separated flows (Table 1).

Table 1: Comparison of grid resolutions in viscous wall-unit

| Case | $\Delta x^+$ | $\Delta y^+$ | $\Delta z^+$ | $N$ ($z^+ < 9$) | Class |
|---|---|---|---|---|---|
| Spalart and Strelets (2000) | 20 | 6.7 | 1.0 | 10 | DNS |
| Alam and Sandham (2000) | 20.7 | 6.2 | 0.9 | 16 | DNS |
| Cadieux et al. (2014) | 26.4 | 27.5 | 1.0 | - | LES-NWR |
| Present study | 8.3 | 4.6 | 0.028 | 26 | HiLES |

LES-NWR (LES with Near-Wall-Resolution); HiLES (High-resolution Implicit LES); $N$ (number of grid points within nine wall units)

In the calculation of the viscous wall-unit above, the maximum value of time-averaged bottom friction coefficient $C_f$ has been used. Taking always into account that the high-order spectral filters identified above leave undamped the upper 50% of Fourier & Legendre modes, the study under consideration is still very competitive with a DNS, particularly in terms of the near-wall region which is actually far more resolved than what is achieved in published DNS. There are 17 vertical grid points within the viscous sublayer ($z^+ < 5$) and 125 points in viscous wall region ($z^+ < 50$). Such a high resolution obviates the need for wall-modelling.

## 3. Results

### 3.1. No Background Current

The first case simulated is that of a wave propagating into quiescent water, i.e. with no background current present. The adverse pressure gradient under the rear edge of the wave

generates a near-bed flow reversal, leading to BBL separation immediately upstream of the wave trough. Curiously, the separated BBL never reattaches to the bed much like what is observed in the laboratory (Carr et al. 2008). On account of this intense reversed flow, the BBL flow trailing it is linearly stable. For the purpose of exploring the potential of subcritical instability, a temporally periodic, along-wave-localized volumetric forcing, conceptually similar to that used by Jones et al. (2008) in their study of a laminar separation bubble over an aerofoil, is introduced near the bed ahead of the wave with amplitude of 5% of the wave phase speed. The forcing-emitted perturbation first diminishes due to the favourable pressure gradient at the wave's leading edge but is amplified after it travels past the wave trough, giving rise to local convective instability. As shown in Figure 2, although the enhanced disturbance is quite coherent in the streamwise direction (left panel, at 3.5 wavelengths downstream) it dissipates further downstream (right panel, at 4.5 wavelengths downstream). When the forcing is deactived, all the disturbances are convected downstream and the original (2D) steady laminar flow reappears ; no self-sustained near-bed turbulent wake is observed.

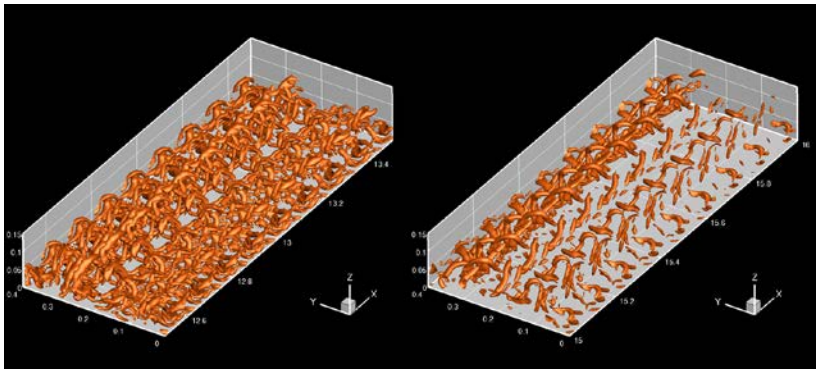

Figure 2: Evolution of forced disturbance downstream of the wave for the no background current case. Shown are isometric surfaces of $\lambda_2$ as defined by Jong and Hussain (1990). Left and right panels correspond to streamwise windows of $12.5 \leq x/H \leq 13.5$ and $15 \leq x \leq 16$ for $0 \leq z/H \leq 0.15$

### 3.1. Oncoming Background Current

The absence of any self-sustained near-bed turbulent wake in the no-background current case motivates the introduction of an oncoming background current. As such, the bottom shear of the oncoming current alters the structure of the BBL in the rear of the wave, forcing it to reattach and giving rise to a separation bubble. The separation bubble then undergoes a spontaneous, self-sustained global instability (Figure 3, top panel), which is the primary requirement for self-sustained turbulence to eventually form in the associated near-bed vortex wake. In this study, a uniform current is chosen with a velocity of 50% of the ISW phase speed in the no current case. To maintain the no-slip condition at the bed, the current was set to decrease to zero at the bed across the lower 4.7% of the total water column. A Blasius profile is used for the near-bed current shear profile. The choice of such a profile is motivated by numerical, not physical considerations, as the spectral flow solver requires a differentiable current profile for clean, numerical-noise-free simulations. One may of course argue that the BBL global instability properties are highly dependent on the magnitude and shape of the near-bed component of the background current. However, the investigation of such a parametric dependence is out of the scope of this study, simply due to computational cost. To this end, it is emphasized that, in addition to a few million CPU hours spent configuring test runs, 2 million CPU hours have been dedicated to date on the oncoming current production run. Consequently, we are still in the middle of the full anticipated time integration and, thereby, only preliminary results are reported here.

Figure 3 shows a series of snapshots of spanwise perturbation vorticity sliced at the mid span of the domain. Three-dimensional details of the first two panels of this figure are given in Figure 4. Initially 2-D Kelvin-Helmholtz-like billows are shed by the rear end of the separation bubble. Neighboring vortices then pair and merge into larger vortices. The larger vortices rotate over the bed, interacting with it, rolling up opposite sign vorticity on the bed. During this interaction process the outer "shell" of a vortex becomes distorted, degenerating into streamwise vortices (streaks) that wrap around the rolling vortex. The coherent (two-dimensional) vortical structure then quickly breaks down into groups of small eddies which constitute intense patches of turbulence, several of which burst upward reaching close to the top boundary. The above vortex-wall interaction generates a local bed shear stress which is a considerably larger than that found in the turbulent BL region further downstream (not shown here). The very fine-scale nature of this near-wall transition process is what necessitates a large, non-trivially expensive, number of grid points to correctly simulate the associated physics. Finally, note that no artificial noise or disturbances are seeded into the BBL to initiate and maintain the instability and subsequent turbulence ; the turbulent near-bed wake in the ISW-induced BBL is self-generated and self-sustained.

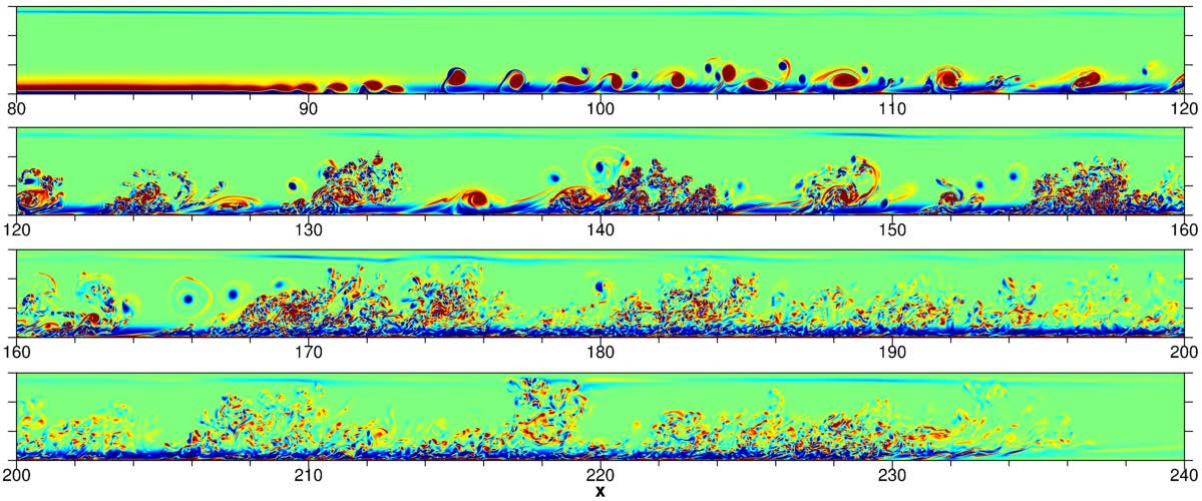


Figure 3: Instantaneous spanwise perturbation vorticity at the mid-span for oncoming current case. Dimensional units of length are used. The wave trough is located at $x$ = 60m.

Closer examination of the middle panel of Figure 4 reveals a three-dimensional intrinsic instability mode that is initiated in the shear layer in the separation bubble. This eigenmode has a wavelength of 1.5$m$, which is full span of the computational domain, and is coupled with the primary, two-dimensional shear instability. This intrinsic spanwise eigenmode has two-pole (positive/negative) spanwise velocities similar to the modal structure of elliptic instability of a strained vortex (e.g., Waleffe 1990). The transverse eigenmode is subsequently trapped in the shed vortices, grows in time, and bends the vortex core. However, the aforementioned wall-vortex instability is strongly nonlinear and has a much faster growth rate, enough to overpower the instability of the transverse eigenmode.

Figure 5 shows the vortical structure of the turbulent wake about 5-wavelengths (top) and 6.5-wavelengths (bottom) downstream of the ISW. The contour of the vertical velocity is also rendered to the isometric surfaces of the vortex filaments. It is clear from the picture that the turbulent region has pairs of upwelling (red) and downwelling (blue) velocity clouds, which are effectively signatures of the preceding (young) two-dimensional billows. However, such distinction is nearly lost in the additionally developed, nearly homogenized turbulent region

further downstream ($x$ > 15 to 16$H$). Closer inspection of the turbulent coherent structure (not shown here) reveals numerous hairpin-type vortices and streamwise streaks attached to the bed, which are very similar to structures of canonical flat-plate turbulent boundary layers.

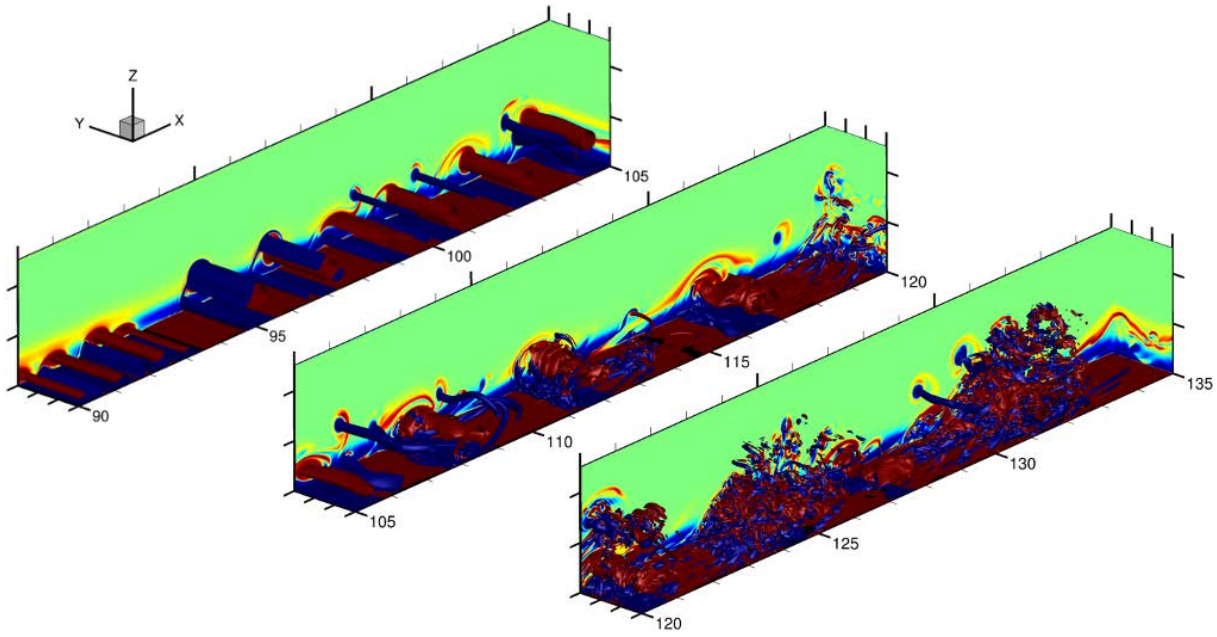


Figure 4: Isometric views of instantaneous spanwise perturbation vorticity over transition region, corresponding to the top two panels of Figure 3.

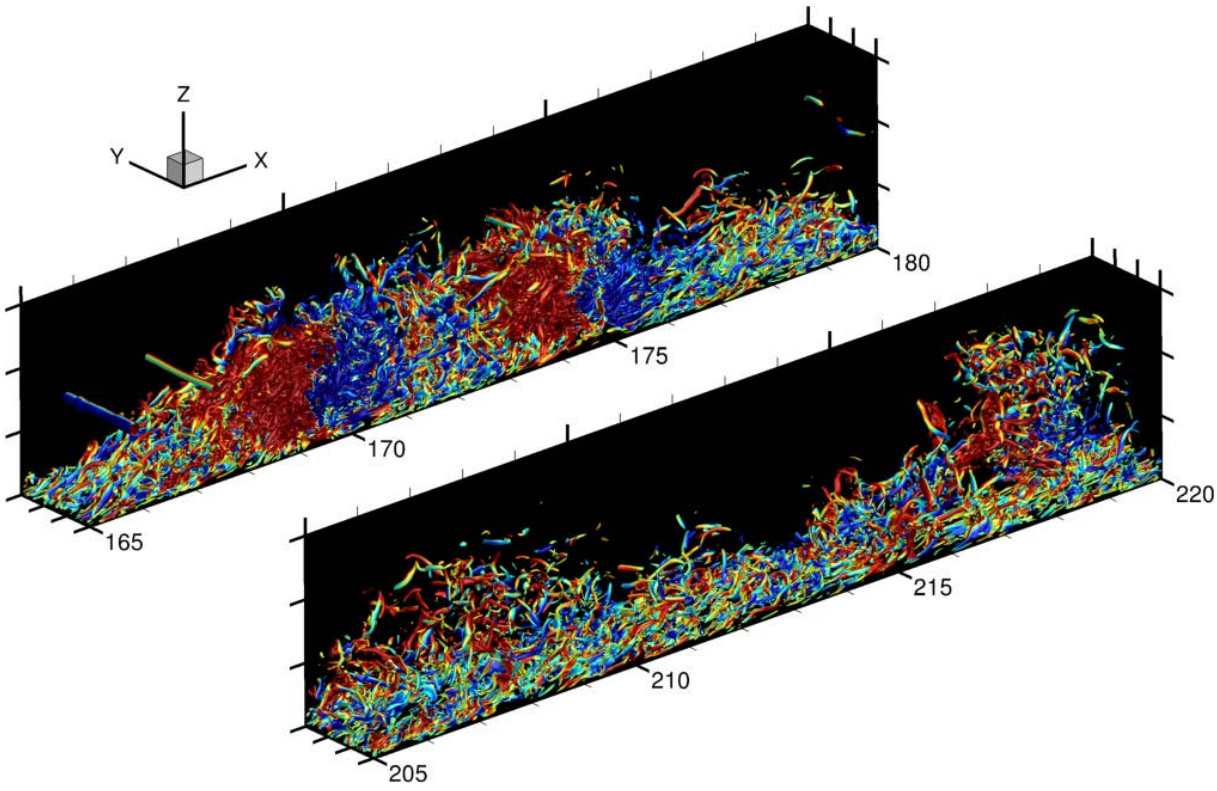


Figure 5: Votical structure of turbulent region. Shown isometric surface of $\lambda_2$ defined by Jong and Hussain (1990) rendered by vertical velocity ranging from -0.11$c_0$ (blue) to +0.11$c_0$ (red).

Figure 6 shows some first quantitative results: the displacement thickness ($\delta$) Reynolds number $Re_\delta$, the momentum thickness ($\theta$) Reynolds number $Re_\theta$, the shape factor $H$ ($=\delta/\theta$ ; here $H$ does not denote the total depth) and the bed friction coefficient $C_f$ of the time-averaged flow as functions of the streamwise coordinate $x$ (this is still preliminary data, averaged over 300 samples only). $Re_\theta$ ranges from 1,500 to 2,000 in the turbulent region up to 6.2 wavelengths downstream of the wave, yet the shape factor nearly converges to a constant value $H\approx1.4$ which is close to that of the zero-pressure gradient flat-plate turbulent boundary layer ($H$=1.3-1.4). It should be noted here that ISW induces a pressure gradient only under the wave and zero pressure gradient elsewhere. The friction coefficient compares favorably to Ludweig and Tillman's skin friction law of the zero-pressure gradient turbulent BL, as given by $C_f = 0.246\times10^{-0.678H}Re_\theta^{-0.268}$. Note that this comparison is valid only in the region of turbulent BBL where the vortical structure is nearly homogenized, i.e. for $x$ > 170 or 180 (see Figure 4 lower panel).

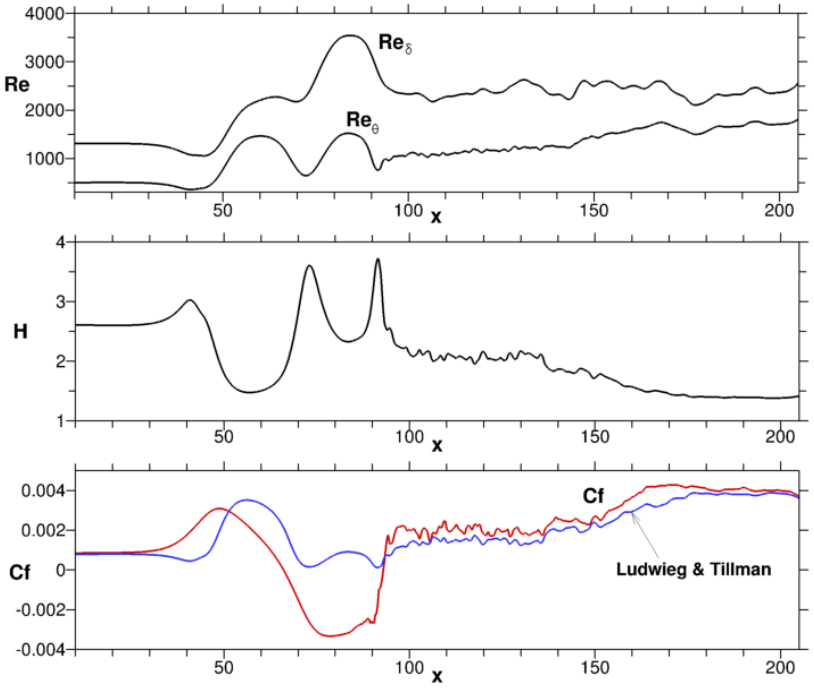


Figure 6: Bounday layer Reynolds numbers $Re_\delta$ and $Re_\theta$, shape factor H and bed friction coefficient $C_f$.

## Discussion

The need for near-bed volumetric forcing to generate near-bed vortex shedding in the no-current case suggests caution in regarding any associated instability as global. Moreover, it indicates that laboratory observations of similar shedding patterns are likely to be linked to the presence of non-negligible bottom roughness and imperfections/asymmetries in the wave generation mechanism (Carr et al. 2008 ; Aghsaee and Boegman 2015). It is also questionable that actual turbulence is attained in the no-current case for the Reynolds numbers considered here and in the laboratory. On the contrary, in the oncoming current case, the complex transition downstream of the separation bubble in the ISW rear gives rise to significant fully developed turbulence, which appears to carry signatures of the transition a large distance downstream. Determination of the downstream distance from the wave trough where signatures of the vortex shedding persist is the topic of ongoing work. A more quantitative characterization of this boundary layer, which entails running the LES even longer to accumulate even greater number of snapshots of the turbulent BBL in statistically steady

state, is also underway. The latter will involve a quantification of near-bed energetics with an emphasis on bottom shear stress fields and the resulting drag on the propagating ISW.


## Acknowledgements

Prof. Larry Redekopp, who originated the idea of global instability under ISWs, is thanked for numerous illuminating conversations and endless encouragement. Numerous other colleagues, namely Profs. Marek Stastna, Magda Carr and Luis Parras, have also shared multiple enlightening discussions. Support from ONR grant N00014-11-1-0511 and NSF-CAREER award OCE-0845558 is acknowledged. Computational time was provided through the U.S. DoD HPC program's Open Research Systems.


## References


Alam, M. and Sandham, N. D. (2000) Direct numerical simulation of 'short' laminar separation bubbles with turbulent reattachment. *J. Fluid Mech.* 403, 223–250.

Aghsaee, P., Boegman, L., Diamessis, P.J. and Lamb, K.G. (2012). Boundary layer separation and vortex shedding beneath internal solitary waves. *J. Fluid Mech.* 690, 321-344.

Aghsaee. P. and Boegman, L. (2015). Experimental investigation of sediment re-suspension beneath internal solitary waves of depression. *J. Geophys. Res.* 120(5), 3301-3314.

Bogucki, D., Redekopp, L. G. and Barth, J. (2005). Internal solitary waves in the Coastal Mixing and Optics Experiment 1996: Multimodal structure and resuspension. *J. Geophys. Res.*, 110(C2):Art. No. C02024.

Cadieux, F., Domaradzki, J. A., Sayadi, T., Bose, S. and Duchaine, F. (2014) DNS and LES of separated flows at moderate Reynolds numbers, *J. Fluids Eng* 136(6), 060902.

Carr, M, Davies, P. A. and Shivaram, P. (2008) Experimental evidence of internal solitary wave-induced global instability in shallow water benthic boundary layers. *Phys. Fluids*, 20:Art. No. 0666031.

Diamessis, P.J., Domaradzki, J.A., and Hesthaven, J.S., (2005). A spectral multidomain penalty method model for the simulation of high Reynolds number localized incompressible stratified turbulence. *J. Comp. Phys.*, 202, 298-322.

Diamessis, P. J. and Redekopp, L.G., (2006). Numerical investigation of solitary internal wave-induced global instability in shallow water benthic boundary layers. *J. Phys. Oceanogr.*, 36(5), 784–812.

Dunphy M, C. Subich, M. Stastna, (2011), Spectral methods for internal waves: indistinguishable density profiles and doublehumped solitary waves. *Nonlin. Proc. in Geoph.*, 18(3):351–358.

Harnanan, S., Soontiens N. and Stastna, M. (2015). Internal wave boundary layer interaction: A novel instability over broad topography. *Phys. Fluids*, 27(1); Art. No. 016605.

Jeong, J. and Hussain, F., (1995). On the identification of a vortex. *J. Fluid Mech*., 285, 65-94.

Moum, J. N., D. M. Farmer, E. L. Shroyer, W. D. Smyth, L. Armi, (2007). Dissipative losses in nonlinear internal waves propagating across the continental shelf. *J. Phys. Oceanogr.*, 37, 1989–1995.

Lamb, K. G. and Wan, B. (1998) Conjugate flows and flat solitary waves for a continuously stratified fluid. *Phys. Fluids* 10(8), 2061–2079.

Jones, L. E., Sandberg, R. D. and Sandham, N. D. (2008) Direct numerical simulations of forced and unforced separation bubbles on an airfield at incidence. *J. Fluid Mech.* 602, 175–207.

Quaresma, L.S., Vitorino, A., Oliveira, A. and da Silva, A. (2007) "Evidence of sediment resuspension by nonlinear internal waves on the western portuguese mid-shelf," *Marine Geology* 246, 123.

Reeder, D., B. Ma, and Y. J. Yang, (2010). Very large subaqueous sand dunes on the upper continental slope in the South China Sea generated by episodic, shoaling deep-water internal solitary waves, *Mar. Geol*., 279, 12-18.

Soontiens, N., Stastna, M. and Waite M. (2015). Topographically generated internal waves and boundary layer instabilities *Phys. Fluids*, 27(8); Art. No. 086602.

Spalart, P. R. and Strelets, M. K. (2000) Mechanisms of transition and heat transfer in a separation bubble. *J. Fluid Mech*. 403, 329–349.

Stastna, M. and K. G. Lamb, (2008). Sediment resuspension mechanisms associated with internal waves in coastal waters. *J. Geophys. Res.*, 113: C10016.

Waleffe, F. (1990) On the three-dimensional instability of strained vortices. *Phys. Fluids* A 2(1), 76-80.